JOURNAL OF MATERIALS SCIENCE 22 (1987) 202–206

Rapidly solidified microstructure of Al–8Fe–4 lanthanide alloys

Y. R. MAHAJAN, YOUNG-WON KIM*, F. H. FROES
*Air Force Wright Aeronautical Laboratories, Materials Laboratory, AFWAL/MLLS, and *Metcut-Materials Research Group, P.O. Box 33511, Wright-Patterson Air Force Base, Ohio 45433, USA*

Al–8Fe and Al–8Fe–4RE (cerium, erbium, neodymium and gadolinium) alloys were rapidly solidified by the melt-spinning technique. The microstructure and phases of alloy ribbons were studied using optical metallography, SEM, TEM and X-ray diffraction techniques. The study has indicated that RE additions to Al–8Fe: (1) result in formation of an increased amount of fine microstructure region, (2) increase the hardness and stability, and (3) generally suppress the formation of needle-type Al_3Fe compounds by substituting them with globular $Al_{10}Fe_2RE$ compounds. The addition of gadolinium appears to produce the best results.

1. Introduction

Rapidly solidified (RS) Al–8Fe alloys with the addition(s) of the ternary or quarternary elements such as cerium, nickel, cobalt, zirconium, molybdenum, vanadium, etc. [1–9] have offered excellent potential for elevated temperature applications. In particular, the Al–Fe–Ce alloy system has shown great promise due to its excellent high-temperature tensile strength with moderate ductility, reasonable thermal stability, and good creep properties [1, 4, 5]. It has been speculated that these beneficial properties of Al–Fe–Ce alloys are largely derived from the influence of cerium in reducing embrittlement and promote stability in Al–Fe alloys by suppressing Al_xFe formation in favour of a ternary (Al–Fe–Ce) phase [1, 5, 10]. The purpose of the present work is to see if similar effects, specifically microstructure and stability, can be obtained when Al–8Fe alloys having other rare earth elements (erbium, neodymium, gadolinium) are rapidly solidified. Similar effects virtually indistinguishable from one element to another may be expected because Al–RE (where RE = rare earth) binary systems form simple eutectic phase diagrams and Al–Fe–RE ternary phase diagrams [11–14] exhibit almost the same solid phase fields. Preliminary experiments on melt-spun ribbon alloys of Al–8Fe–4Ce and Al–8Fe–4Gd show, however, that there are differences in overall microstructures and solidification characteristics. These differences were identified and characterized using phase relations, annealing behaviour, and phase analysis.

2. Experimantal procedure

One binary alloy Al–8Fe and four ternary alloys Al–8Fe–4RE (RE = cerium, erbium, neodymium and gadolinium) were prepared into button forms by repeated arc melting. The alloy buttons were then induction melted in a quartz crucible to a superheat of $\sim 100°C$ and ejected through a nozzle by applying argon gas pressure onto a rapidly rotating (surface velocity = $20\,m\,sec^{-1}$) water-cooled copper wheel. The average thickness of the melt-spun ribbon was about 50 μm. The nominal composition and the actual composition determined by chemical analysis after melt-spinning are listed in Table I. The ribbons were isochronally annealed in vacuum for 1 h at various temperatures ranging from 100 to 600° C. The microhardness (Knoop) measurements on ribbons annealed at relatively low temperatures were taken on the optically featureless zone of the longitudinal section of the ribbon. For the ribbons annealed at high temperatures, extreme care was taken to locate the originally featureless zone. The ribbon microstructure was studied by optical metallography, scanning electron microscopy (SEM), and transmission electron microscopy (TEM) techniques. X-ray diffraction was used to identify phases on the chill-side surfaces of the ribbons in both as-melt spun and 600° C annealed conditions.

3. Results and discussion

3.1. As-melt spun microstructure

Fig. 1 shows typical microstructures of longitudinally cross-sectioned ribbons for Al–8Fe (a), Al–8Fe–4Ce (b), Al–8Fe–4Nd (c), and Al–8Fe–4Gd (d). Fine microstructure regions (F) present on the wheel side of ribbons do not etch, distinguishing themselves from the etch-sensitive, coarse regions (C) that surround these F regions. The microstructure is coarsest on the air side of ribbons as is evidenced by primary compounds present in Fig. 1a or by more severe etching

TABLE I Chemical composition, (wt%)

Nominal	Actual
Al–8Fe	Al–8.16Fe
Al–8Fe–4Ce	Al–7.82Fe–4.03Ce
Al–8Fe–4Nd	Al–8.57Fe–4.56Nd
Al–8Fe–4Gd	Al–7.60Fe–4.20Gd
Al–8Fe–4Er	Al–7.55Fe–4.22Er

0022–2461/87 $03.00 + .12

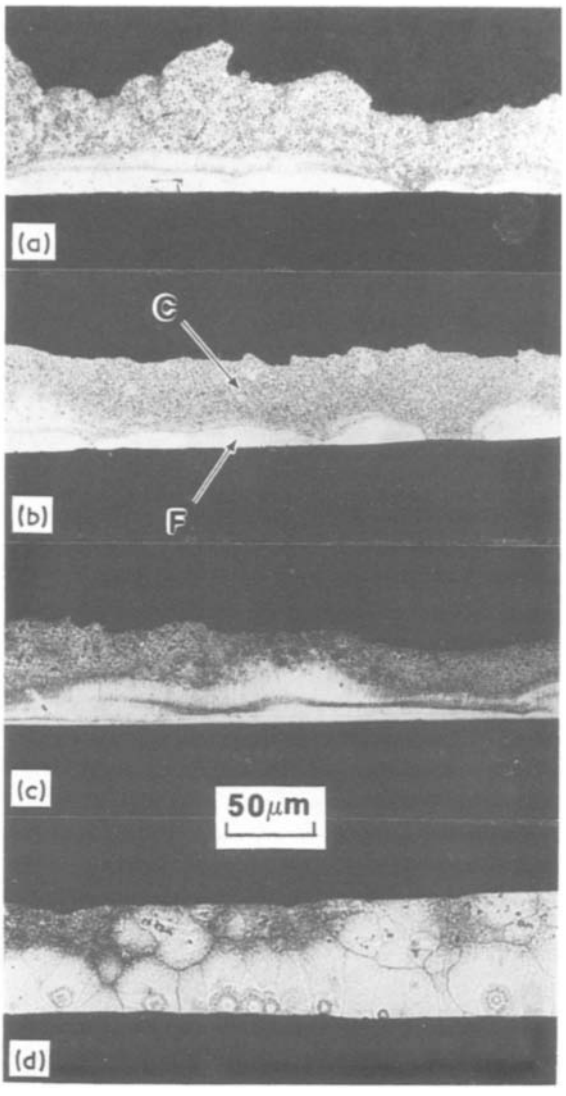

Figure 1 Optical micrographs of (a) Al–8Fe, (b) Al–8Fe–4Ce, (c) Al–8Fe–4Nd, and (d) Al–8Fe–4Gd as-melt spun alloy ribbons (longitudinal cross-section) showing fine (F) and coarse (C) regions.

in Fig. 1b. The F regions are continuous (Fig. 1c) longitudinally, or sometimes discontinuous (Figs 1a and b). It is noted that the situation in Al–8Fe–4Er is similar to that of Al–8Fe–4Ce (Fig. 1b).

The microstructure of the wheel side surface provides valuable information on the solidification characteristics of Al–8Fe–4Ce (Fig. 2a) and Al–8Fe–4Nd (Fig. 2b) alloy ribbons. The alloy melt starts to solidify at each contact point with the wheel surface, first forming a predendritic zone (F) with radially propagating cellular type dendrites. When the predendritic regions do not meet each other, they are separated by the coarse regions (C) that are typically of dendritic microstructure with (Fig. 2b) or without (Fig. 2a) primary compounds. The formation of primary compounds on the air-side surface was also observed in Al–Co alloy ribbon [15]. The separation of F regions by C regions on the wheel side is also seen cross-sectionally in Fig. 1, as was discussed. The predendrites are generally oval shaped and elongated to the longitudinal (or spinning) direction, Fig. 2a. Long F regions occasionally observed as shown in Fig. 1a are the result of extensively elongated predendrites (top left, Fig. 2a)

The alloy Al–8Fe–4Gd ribbon shows quite different overall features, Fig. 1d, although the detailed microstructure is similar as will be shown later. The F regions are continuous along the wheel side of ribbon indicating a good contact between the alloy melt and the wheel, which results in more nucleation sites or predendritic zones. The nucleation sites for solidification are also evident in many cases in the cross-section. Nucleation in the melt is associated with primary compound particles in general, but there are cases without any primary compound involvement. Each nucleation forms a grain sharply bounded by adjacent grains and the grain size ranges from 5 to 35 μm, Fig. 1d. Although some coarse regions and primary compound particles are observed on the air side of ribbon, alloy Al–8Fe–4Gd ribbon reveals RS microstructure that is the finest and the most uniform in average of all the alloys investigated.

Fig. 3 shows TEM microstructure that is typical of Al–8Fe ribbon (a and b) and common in Al–8Fe–RE alloys (c and d). Fig. 3a shows the transition region from region F to C (see Fig. 1a) that was solidified to dendritic microstructure with a cooling rate of 10^5 to 10^6 K sec^{-1} according to the arm spacing or cell to cell distance. Details of slowly cooled C regions

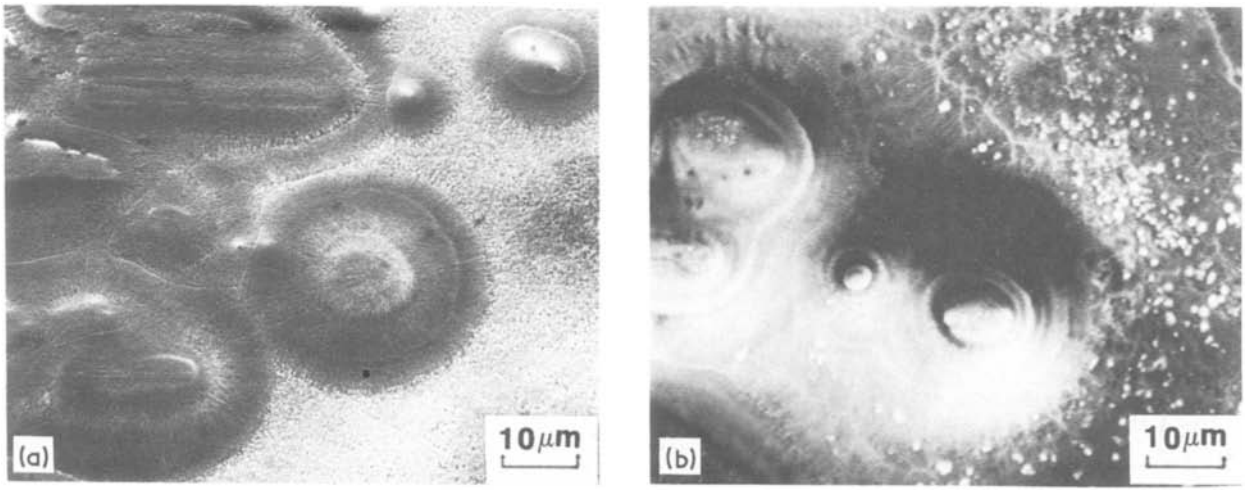

Figure 2 The wheel side surfaces of as-melt spun (a) Al–8Fe–4Ce and (b) Al–8Fe–4Nd alloy ribbons showing predendritic regions and coarse regions.

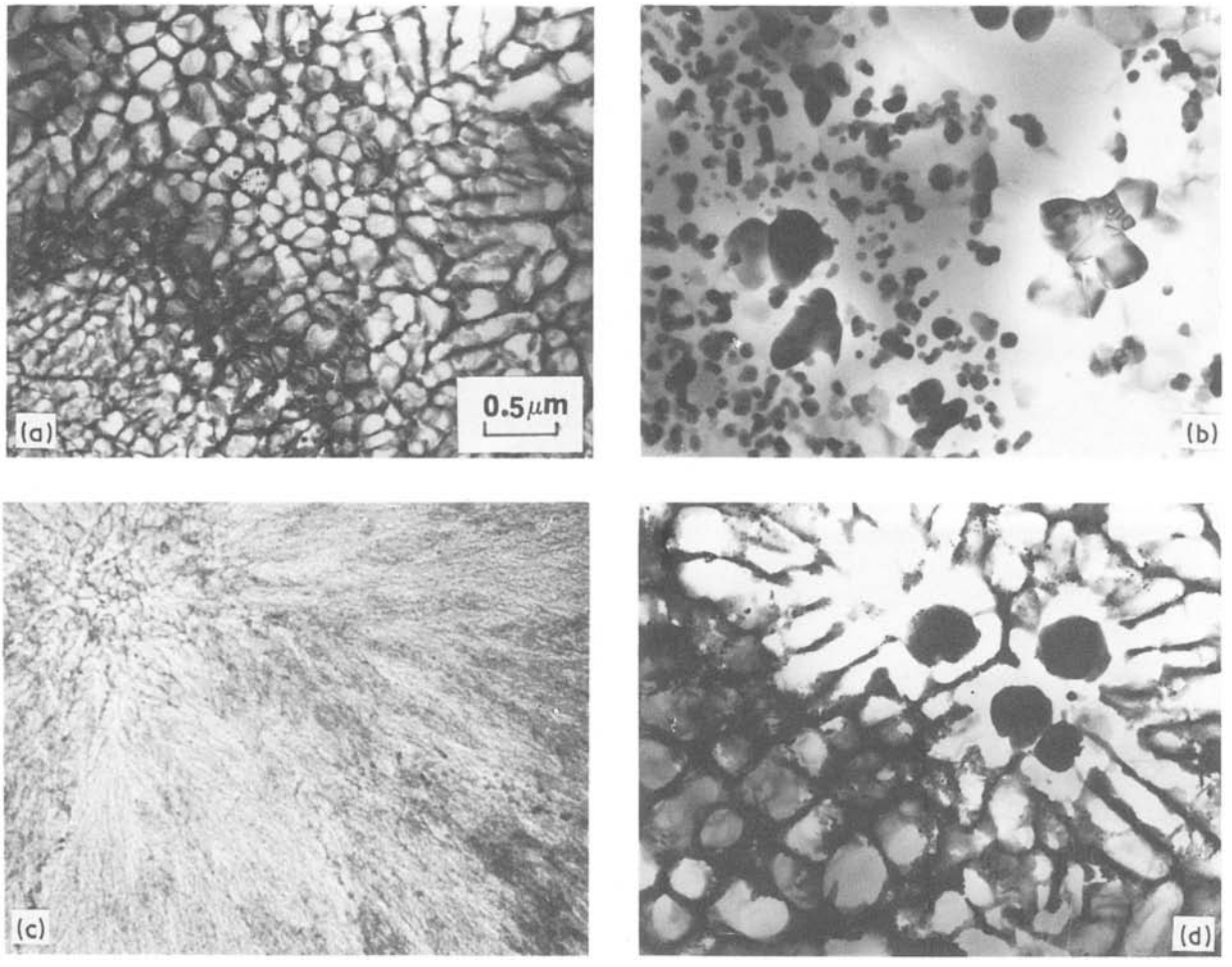

Figure 3 TEM micrographs of as-melt spun Al–8Fe (a and b) and Al–8Fe–4RE (c and d) alloy ribbons, showing rapidly cooled regions (a and c) and slowly cooled regions (b and d).

(see Fig. 1a) are shown in Fig. 3b that reveals large primary compounds and eutectic microstructure, in addition to dendritic microstructure, typical of hypereutectic alloys. Fig. 3c shows fine microstructure in the F regions near the nucleation centre (top left) commonly found in Al–8Fe–4RE alloy ribbons. According to the arm spacing ($\sim 0.1\,\mu m$) of the cellular type dendrites radially oriented around the nucleation centre, the typical cooling rate is estimated to be in the range of 10^8 K sec^{-1}. The primary compound particles in Fig. 3d nucleate dendrites of α-phase in equiaxed form in many cases. No eutectic microstructure was found in any of Al–8Fe–4RE alloys.

3.2. Effect of annealing

Fig. 4 shows the effect of isochronal annealing on the hardness of F regions in the ribbon alloys. As-melt spun hardness varies widely from KHN of 195 for Al–8Fe and Al–8Fe–4Ce to over 300 for Al–8Fe–4Gd, with Al–8Fe–4Nd and Al–8Fe–4Er (not shown here) having intermediate hardness values. This indicates that the addition of rare earth elements to Al–8Fe generally increases the hardness of fine microstructure regions.

All the alloys show age hardening upon isochronal annealing with the peak hardnesses at temperatures between 200 and 300° C. Alloy Al–8Fe–4Gd shows a slight decrease in hardness around 100° C, that is followed by a moderate, slow hardness increase up to ~250° C. The softening after the peak is very slow up to ~400° C, indicating that this alloy is the most stable at least up to this temperature. Alloy Al–8Fe–4Nd shows generally a similar trend except for the

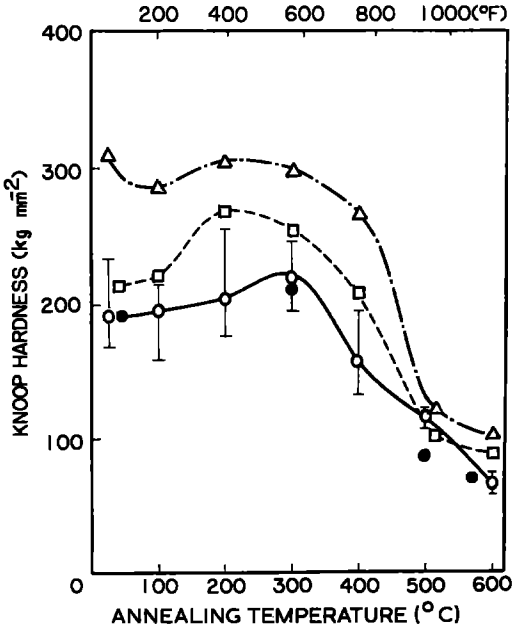

Figure 4 Knoop hardness number plotted against isochronal annealing temperature for the fine regions in melt spun Al–8Fe and Al–8Fe–4RE alloy ribbons. (△) Al–8Fe–4Gd, (□) Al–8Fe–4Nd, (○) Al–8Fe–4Ce, (●) Al–8Fe.

TABLE II Phases identified by X-ray

Alloy	As-melt spun	After 600° C/1 h
Al–8Fe	Al_6Fe (m) Al_3Fe (vs)	Al_3Fe (l)
Al–8Fe–4Ce	Al–Fe–Ce* (s) Al_6Fe (s)	Al_3Fe (l) $Al_{10}Fe_2Ce$† (l)
Al–8Fe–4Er	Al–Fe–Er* (s) Al_6Fe (vs)	Al_3Fe (m) $Al_{10}Fe_2Er$‡ (l)
Al–8Fe–4Nd	Al–Fe–Nd* (s) Al_6Fe (vs)	Al_3Fe (m) $Al_{10}Fe_2Nd$‡ (l)
Al–8Fe–4Gd	Al–Fe–Gd* (vs) Al_6Fe (vvs)	$Al_{10}Fe_2Gd$‡ (l) Al_3Fe (s)

vvs = extremely small amount; vs = very small; s = small; m = medium; l = large amount.

*These ternary compounds were not identified but they appear to be isostructural.

†The presence of $Al_{10}Fe_2Ce$ has been recently identified positively [19].

‡These are isostructural to $Al_{10}Fe_2Ce$.

more pronounced age hardening. Both Al–8Fe–4Ce and Al–8Fe show the age hardening peak at a higher temperature but rapid softening immediately after the peak.

The softening at temperatures higher than 400° C is quite dramatic, with the more severe softening for initially harder alloys. At around 500° C, the hardness decrease slows down, possibly except for Al–8Fe–4Ce which shows an accelerated hardness drop. It is noteworthy that Al–8Fe–4Gd maintains the highest hardness through the isochronal annealing.

Fig. 5 shows the SEM microstructures of Al–8Fe (a), Al–8Fe–4Ce (b), and Al–8Fe–4Gd (c) after an annealing at 600° C for 1 h. The intermetallic compounds are substantially coarsened to the size range from 0.2 to $\sim 3\,\mu m$, explaining why the hardness of the alloys is reduced to half or lower of the original hardness after this annealing (see Fig. 4). The morphology of compounds varies widely depending upon alloy. In alloy Al–8Fe, they are either needle-type or globular or occasionally faceted. In Al–8Fe–4Ce, the situation is similar but the compounds are more globular than needle-like. In Al–8Fe–4Gd, the compounds are not only smaller overall but they are globular or spherical in almost all cases. It is noted that the microstructure of Al–8Fe–4Er is similar to that of Al–8Fe–4Ce and that of Al–8Fe–4Nd is close to that of Al–8Fe–4Gd.

3.3. Phases

All the phases present in the as-melt spun condition and after the 600° C/1 h annealing were analysed using X-ray diffraction patterns and existing data [14, 16–18]. Table II lists all the phases detected.

In the as-melt spun condition, the overall amount of intermetallic compounds is reduced by adding rare earth elements, gadolinium being the most effective. The reduction with gadolinium addition is clearly seen in Al–8Fe–4Gd, Fig. 1. Another feature is that the rare earth addition virtually eliminates the formation of Al_3Fe-type compounds but results in the formation of Al–Fe–RE compounds. The ternary compounds appear to be isostructural according to the strong peaks but have not been identified.

After the 600° C/1 h annealing, Al_3Fe was the only compound detected in Al–8Fe. In addition to Al_3Fe, Al–8Fe–4RE alloys contain $Al_{10}Fe_2RE$ type compounds which are isostructural to $Al_{10}Fe_2Ce$ [19]. These ternary compounds are generally globular or spherical compared to the needle-shaped Al_3Fe [4, 5, 19]. The increased amount of this compound in the order of cerium, erbium, neodymium and gadolinium (Table II) explains the increased amount of globular compounds in Fig. 5.

3.4. Effect of rare earth addition

The tendency to form more fine regions with RE additions may be explained by the possible lowering of the liquidus that reduces the liquid–solidus temperature range ($\Delta T_{LS} = T_L - T_S$). This will reduce the segregation during cooling. This reduction of ΔT_{LS} is possible because of high eutectic composition (C_E) of Al–RE binaries. For example, the C_E for Al–Ce and Al–Gd and 16 and 24 wt %, respectively, while C_E of Al–Fe is only 1.8 wt %.

The increased hardness of Al–8Fe–4RE in the

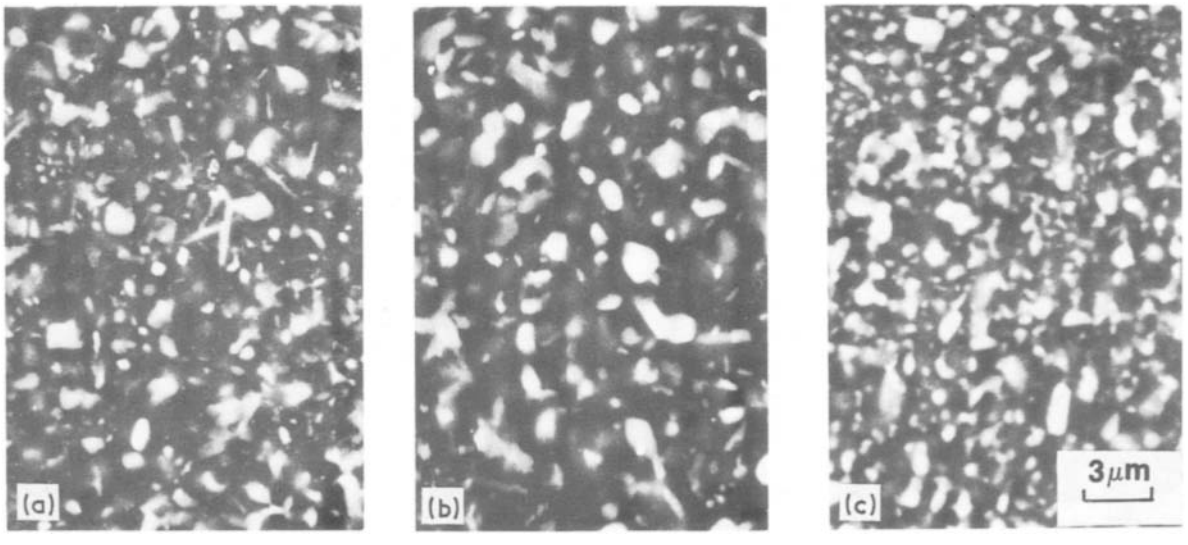

Figure 5 SEM microstructures of (a) Al–8Fe, (b) Al–8Fe–4Ce, and (c) Al–8Fe–4Gd alloy ribbons (longitudinal cross-section) after annealing at 600° C for 1 h.

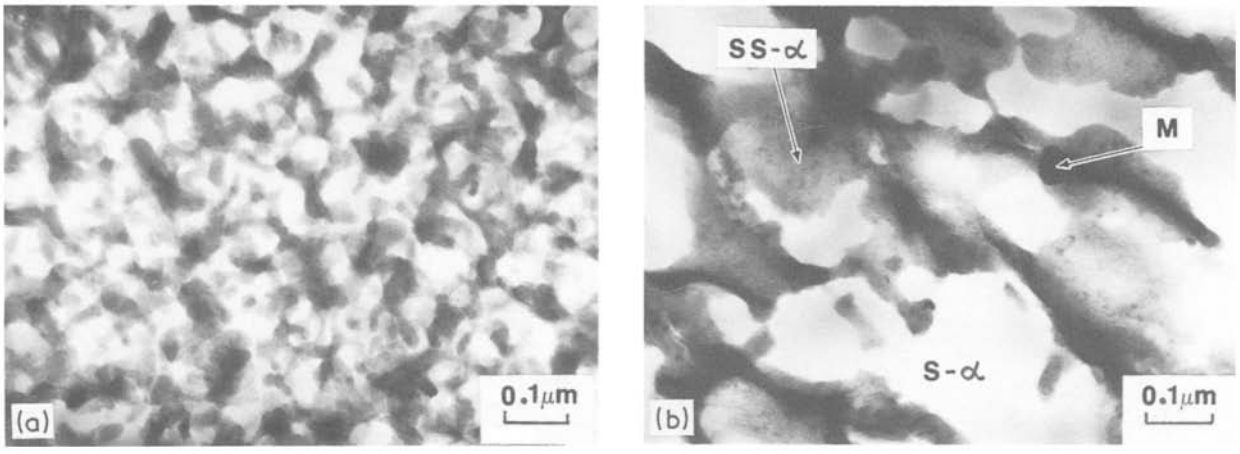

Figure 6 TEM micrographs of as-melt spun Al–8Fe–4Gd alloy ribbon. (a) Fine region, (b) coarse region, showing saturated α-Al (S-α), supersaturated α-Al (SS-α) and interdendritic metastable compounds (M).

order cerium, neodymium and gadolinium can be explained in terms of the formation of an increased amount of fine region, which means increased suppression of solute segregation during cooling and the effective refining of segregated solutes to the finest possible compound particles. This is reflected in Table II and also is shown in Fig. 6 for Al–8Fe–4Gd as the most effective case. In Fig. 6 showing dendritic cells in relatively coarse region cooled at $\sim 10^6$ K sec^{-1} α-Al cells (S-α) are surrounded by supersaturated α-Al (SS-α). Dark spots in the supersaturated α region are mostly ternary intermetallic compounds (M), the size of which is not greater than 0.1 μm. Many of these compounds are so small that they are not detected by X-ray diffraction. This means that the very small amount of compounds detected in as-melt spun Al– 8Fe–4Gd (Table II) does not necessarily indicate almost all the solutes in solid solution.

The disappearance of needle-shaped compounds in Al–8Fe–4RE especially in Al–8Fe–5Gd means that the RE addition forms ternary compounds by eliminating needle-type Al_3Fe compounds. This effect, however, is not obvious in the as-melt spun condition but appears when annealed, Fig. 5. Since the ternaries formed after annealing are isostructural to $Al_{10}Fe_2Ce$ (Table II), however, it is difficult to understand why gadolinium eliminates Al_3Fe. One explanation is that in Al–8Fe– 4Gd, the ternary may be in an $Al_{10}Fe_2$ (gadolinium, iron) form eliminating Al_3Fe more effectively.

4. Conclusions

In the study of rapidly melt spun alloy ribbons of Al–8Fe and Al–8Fe–4RE (cerium, erbium, neodymium and gadolinium), the following were observed:

1. RE additions result in formation of finer microstructure;

2. RE additions increase the hardness over Al–8Fe and generally increase stability; and

3. RE additions generally suppress the formation of needle-type Al_3Fe compounds, when annealed, by substituting them with globular $Al_{10}Fe_2RE$ compounds. The beneficial effects increase in the order of erbium, cerium, neodymium and gadolinium addition.

Acknowledgements

One of the authors (Y.R.M.) wishes to thank the National Research Council, USA for providing a resident research associateship. This work was partially supported by the Air Force Materials Laboratory under Contract no. F33615-82-C-5078.

References

1. W. M. GRIFFITH, R. E. SANDERS Jr and G. J. HILDEMAN, in "High-Strength Powder Metallurgy Aluminum Alloys", edited by M. Koczak and G. J. Hildeman, (TMS, Warrendale, Pennsylvania, 1982) pp. 209–24.
2. G. THURSFIELD and M. J. STOWELL, *J. Mater. Sci.* **9** (1974) 1644.
3. C. M. ADAM, in "Rapidly Solidified Amorphous and Crystalline Alloys", edited by B. H. Kear, B. C. Giessen, and M. Cohen, (Elsevier, New York, 1982) p. 411.
4. M. E. FINE and J. R. WEERTMAN, Synthesis and Properties of Elevated Temperature P/M Aluminum Alloys, Air Force Office of Scientific Research Annual Report, AFOSR-82-005, November 30, (1984).
5. Y-W. KIM and W. M. GRIFFITH, in "Rapidly Solidified Powder of Aluminum Alloys", ASTM STP 890, edited by M. E. Fine and E. A. Starke Jr (American Society for Testing and Materials, Philadelphia, Pennsylvania, 1986) p. 485.
6. M. S. ZEDALIS, PhD thesis, Northwestern University (1985).
7. K. OKAZAKI and D. J. SKINNER, *Scripta Metall.* **18** (1984) 911.
8. D. J. SKINNER and K. OKAZAKI, *ibid.* **18** (1984) 905.
9. A. K. GOGIA, P. V. RAO and J. A. SEKHAR, *J. Mater. Sci.* **20** (1985) 3091.
10. L. F. MONDOLFO, "Aluminum Alloys: Structure and Properties" (Butterworth, London, 1976) p. 468.
11. O. S. ZARECHNYUK, M. G. MYSKIV and V. R. RYABOV, *Russian Metallurgy* **2** (1969) 133.
12. O. I. VIVCHAR, O. S. ZARENCHNYUK and V. R. RYABOV, *ibid.* **1** (1970) 140.
13. *Idem, Dopov. Akad. nauk URSR* **35** (1973) 1040.
14. O. S. ZARECHNYUK, O. I. VIVCHAR and V. R. RYABOV, *Vestn. Lvov. Univ. (Khim.)* **14** (1972) 16.
15. R. K. GARRETT and T. H. SANDERS, in "Chemistry and Physics of Rapidly Solidified Materials", edited by B. J. Berkowitz and R. O. Scattergood (TMS, Warrendale, Pennsylvania 1983) p. 306.
16. K. ITO, *J. Jpn Inst. Light Metals* **29** (1979) 246.
17. ASTM X-ray Data Card No. 2-1213.
18. I. FELNER and I. NOWIK, *J. Phys. Chem. Solids* **39** (1978) 951.
19. Y-W. KIM, *Met. Trans.* (1986) submitted.

Received 16 December 1985
and accepted 6 May 1986